Velocity Structure of the Benthic Ocean

ERIC D'ASARO[1]

Woods Hole Oceanographic Institution, Woods Hole, MA 02543

(Manuscript received 7 May 1981, in final form 11 January 1982)

ABSTRACT

Velocity measurements in the outer part of the bottom boundary layer on the Hatteras Abyssal Plain are examined for indicators of boundary-layer turbulence. Velocity fluctuations in two frequency bands, near-inertial and high-frequency (1–4 cph), display mixed-layer signatures. The high-frequency velocities measure primarily boundary-layer turbulence. The turbulence, so measured, is modulated on inertial and tidal time scales and extends intermittently to the mixed layer top. The near-inertial velocities are less energetic within the mixed layer than above and, for the dominant clockwise component, the mixed layer leads the interior. Following D'Asaro (1982), this is attributed to turbulent stresses which, consequently, must fill the mixed layer. These observations suggest that the entire bottom mixed layer is at least intermittently turbulent.

1. Introduction

A bottom mixed layer, vertically uniform in potential temperature, salinity and light scattering, is present over large regions of the ocean (Armi and Millard, 1976; Caldwell, 1976; Weatherly and Niiler, 1974; Bowden, 1978). In a recent study Armi and D'Asaro (1980) describe the three-dimensional density structure of the bottom mixed layer over the Hatteras Abyssal Plain in the western North Atlantic (near 28°30'N, 70°30'W). This paper discusses the velocity fluctuations observed in the same study.

The bottom boundary layer has often been modeled as a steady turbulent boundary layer, driven by the interior geostrophic flow, entraining upward into the stratified oceanic interior (Weatherly, 1975; Weatherly and Martin, 1978; Armi, 1977; Thompson, 1973). For a stratification typical of this location, these models suggest a mixed layer height of roughly $0.4\ u^*/f$, where f is the Coriolis parameter, $u^{*2} = \tau/\rho$, and τ is the bottom stress. The observed mixed layers are commonly twice this thickness and sometimes many times thicker (Armi and Millard, 1976; Armi and D'Asaro, 1980). This may be due to a greater depth of turbulent entrainment than is predicted by the present models and/or to convergence of the boundary layer forced by the interior eddy field. A key distinction between these two mechanisms is the distribution of turbulence within the mixed layer. If entrainment is important, the turbulence must extend to the top of the mixed layer, although this, by itself, does not prove that entrainment is occurring. A mixed layer deepened only by mesoscale convergence need not be turbulent throughout its depth. This paper will discuss two indicators of the turbulence distribution within the mixed layer.

This paper will use data from the Benthic Boundary Layer Experiment, described more fully by Armi and D'Asaro (1980), D'Asaro (1980) and Spencer *et al.* (1981). A three-month record of velocity and temperature was obtained from a bottom mooring deployed on the flat Hatteras Abyssal Plain. Average velocity and temperature were recorded every 7.5 min by seven VACM current meters located 15–85 m above the bottom.

Armi and D'Asaro (1980) find an excess of horizontal kinetic energy at 15 and 25 m above the bottom at frequencies above 1 cph, and a deficit of horizontal kinetic energy at these same levels near the inertial frequency (see their Fig. 10). This paper will investigate the distribution of energy in these two bands with respect to the observed mixed-layer structure. The high-frequency velocity fluctuations will be attributed primarily to boundary-layer turbulence (Section 2) and can thus be used to find the distribution of this turbulence within the mixed layer (Section 3). In a companion paper (D'Asaro, 1982) the reduction of inertial energy is shown to be due to turbulent stresses within the mixed layer. The inertial signal thus provides a second measure of the turbulence distribution (Section 4).

One instrumental problem will be important in this analysis. As discussed more fully by Spencer *et al.* (1981) and D'Asaro (1980), a consistent directional bias of 7° clockwise in the instruments at 85 and 45 m relative to those at 65 and 55 m is apparent from

[1] Present affiliation: Applied Physics Laboratory, University of Washington, Seattle WA 98105.

0022-3670/82/040313-10$06.50

early June up to 19 July. This bias disappears on 19 July simultaneously with a rapid rotation of the mooring. The exact cause of these errors is unknown, but they are considerably larger than the 2° VACM direction biases estimated by Bryden (1976).

2. Measurement of boundary layer turbulence

In this section the excess of high-frequency horizontal kinetic energy seen in Fig. 10 of Armi and D'Asaro (1980) is shown to be mostly due to turbulent velocity fluctuations. The distribution of these fluctuations is described in Section 3.

Eastward and northward velocity components from each instrument were high-pass filtered with an 11-element smooth non-recursive filter constructed using an algorithm described by Hamming (1977). This filter has a half-power point at 2 cph and falls with a slope of 8.4 at lower frequencies. Large spikes in the filtered signal caused by instrument rotor stalls have been eliminated in the processing. The velocity signals processed in this way will be called high-pass velocity.

The velocity measured by the VACM sensors (rotor and vane) is vector averaged by the electronics over a 7.5 min interval. The recorded velocity is thus a low-pass filtered version of the velocity measured by the sensors. The combination of this instrumental low-pass filter and the digital high-pass filter described above yields a band-pass filter with a maximum energy transmission of 0.6 and an equivalent 50% energy-transmission pass-band from 2 to 5 cph. If the sensors are perfect, the transfer function between the oceanic velocity and the computed high-pass velocity is described by this band-pass filter.

The spectrum of turbulent velocities expected in the mixed layer will be estimated from data taken in the outer part of a two-dimensional laboratory turbulent boundary layer. The mixed-layer turbulence may be different on account of the influence of both stratification and rotation. Below, the effect of stratification is shown to be weak within the mixed layer; the effect of rotation is largely unknown and presumed small.

The turbulent velocity fluctuations within the boundary layer are expected to scale with u^*. Since u^* is not measured in this experiment it will be estimated using the measured velocity at 15 m. There is generally little speed shear between the various instruments, so the choice of the 15 m instrument is not crucial. The important parameters in this estimate are the bottom roughness and the Reynolds number, $R = U_1\delta/\nu$. An interior velocity $U_1 = 10$ cm s^{-1} and a boundary-layer height of $\delta = 20$ m yield $R = 2 \times 10^6$. For a smooth-wall turbulent boundary layer at this R, a value of $U_1/u^* = 35$ is predicted using the Millikan drag law (Millikan, 1939). Bottom photographs of the Hatteras Abyssal Plain show a flat bottom with occasional 1 cm bumps (Biscaye and Eittreim, 1977). A sand-grain roughness of $l = 1$ cm, which certainly overestimates the effect of these bumps, yields a roughness Reynolds number u^*l/ν of $\sim$30, which is transitional between smooth and rough flow. Hinze's (1959, p. 486) table predicts $U_1/u^* \approx 29$ for this roughness. Csanady's (1967) Ekman-drag formula with $z_0 = \nu/u^*$ yields $U_1/u^* = 34$. A value of $U_1/u^* = 32$ will be used below.

Stable density stratification can strongly influence a turbulent boundary layer and if sufficiently strong can suppress the turbulence completely (Turner, 1973; Arya, 1972). If we assume that the energetic eddies in the outer part of the boundary layer are of the same scale as the boundary layer, $H = 10$ m, and that they have an energy density u^{*2}, a mean velocity $U_1 = 7$ cm s^{-1} gives a kinetic energy of $u^{*2}H \approx 48$ ergs cm^{-2} for $U_1 = 32u^*$. Assuming that these eddies will completely mix any existing stratification $\Delta\rho$ on the scale H will require energy $g(\Delta\rho/\rho)H^2/12$. Using $g(\Delta\rho/\rho) = -0.1\Delta\theta$ and $H = 10$ m, an energy of 4 ergs cm^{-2} is required to mix a temperature gradient of 0.5 m °C(10 m)$^{-1}$, typical of a mixed layer, while 80 ergs cm^{-2} is required to mix the typical 10 m °C(10 m)$^{-1}$ temperature gradient above the mixed layer. Thus the typical stratification within the mixed layer will not strongly affect the boundary-layer turbulence. The stratification above the mixed layer, however, is strong enough to suppress this turbulence. Boundary-layer turbulence is thus expected only within the mixed layer.

The typical horizontal kinetic energy in the outer part of a turbulent boundary layer is u^{*2} (Hinze, 1959, p. 488). Using $U_1/u^* = 32$, the typical turbulent-kinetic-energy level is $10^{-3}\ U_1^2$.

The high-pass energy is sensitive only to velocity fluctuations within a particular range of frequencies. Do the expected turbulent velocity fluctuations have energy in this frequency range? Fig. 1 shows the spectra of downstream and cross-stream velocity fluctuations in the outer part of a laboratory turbulent boundary layer (Bradshaw, 1966). Velocity spectra in the outer part of a laboratory turbulent Ekman layer are similar (Caldwell *et al.*, 1972). The velocity spectra scale with the boundary layer height δ_{995} (defined by the mean speed equal to 99.5‰ of the free-stream speed), and the interior velocity U_1. Fig. 1 shows the high-pass-velocity central frequency of 3.5 cph in these nondimensional coordinates, for a range of mean speeds 5–10 cm s^{-1}, and a 10–20 m range of δ_{995}. The high-pass-velocity central frequency occurs near the peak of the turbulent-kinetic-energy spectrum.

The half-power bandwidth of the high-pass-velocity transfer function is also shown in Fig. 1. Roughly 20% of the turbulent horizontal kinetic energy is contained within this bandwidth. Since this is a 50% transmission bandwidth a measurement of high-pass

energy in the outer part of a turbulent boundary is expected to yield ~10% of the total turbulent horizontal kinetic energy, or $(0.01U_1)^2$.

Fig. 2 shows scatter plots of (high-pass energy)$^{1/2}$ versus speed at 85 m (2a) and 15 m (2b) for the entire 92-day record. Speed is formed from the eastward and northward velocity components filtered with a half-cosine filter of 3 h half-width. The high-pass energy is calculated from the high-pass eastward and northward velocities and is similarly filtered. The 15 m instrument is commonly in a mixed layer, while the 85 m instrument never is. At 15 m the high-pass velocity fluctuations scale with speed, and have a magnitude of $0.01U$. At 85 m the energy is much smaller, displaying a constant level of ~(0.04 cm s^{-1})^2 except at low speeds where the finite threshold of the VACM becomes important. (The energetic points in Figure 2a at 6 cm s^{-1} are associated with a frontlike feature on 4 and 5 June in Fig. 3b.)

The observed high-pass velocity fluctuations appear to be due primarily to boundary-layer turbulence. This interpretation is supported by the following observations: the high-pass velocity is sensitive to velocity fluctuations near the expected spectral peak of boundary-layer tubulence (Figure 1); the observed high-pass energy level is roughly correlated with the lower-frequency velocity (Fig. 2), as expected for boundary layer turbulence; and the high-pass energy level is consistent with the expected turbulent-energy level. Boundary-layer turbulence should be confined to the mixed layer, and be more energetic near the ocean bottom. These features will be seen in Section 3.

Sources of high-frequency velocity fluctuations other than boundary-layer turbulence are also apparent in the data, as will be seen below. The background level of high-pass energy in Fig. 2 suggests an instrumental noise source. Simulations of VACM round-off errors (McCullough, 1975) yield an intrinsic high-pass-velocity noise level of about 0.03 cm s^{-1}. This is comparable to the background energy level in Fig. 2a. Other instrumental sources of high-pass energy, from mooring motion or imperfect sensor response, are possible. These sources, however, should be sensitive only to the velocity field, not to the boundary-layer density structure. As will be seen below, the observed fluctuations show a clear correlation with the boundary-layer density structure.

3. Observed high-pass-velocity structure

The complete record of high-pass energy is displayed in Fig. 3c, with the corresponding potential temperature and 1-day-mean-speed records shown in Figs. 3b and 3a, respectively. A particularly interesting mixed layer occurs from 25 July to 4 August. This period is detailed in Fig. 4 and will be discussed first.

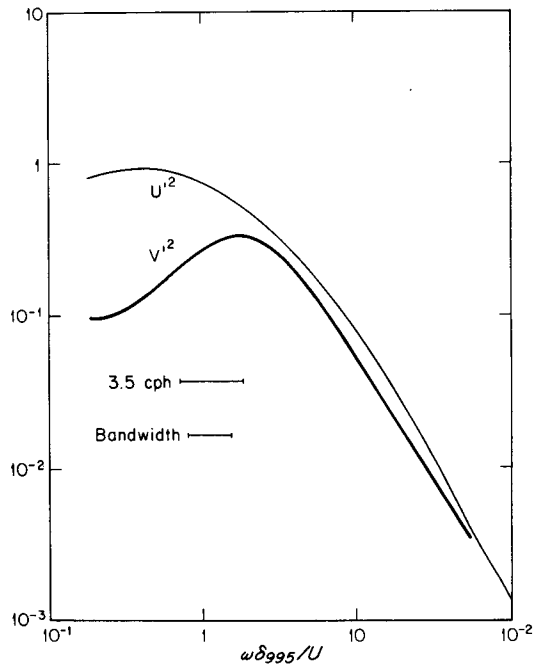

FIG. 1. Spectrum of cross-stream (U') and downstream (V') turbulent velocity fluctuations in a laboratory two-dimensional turbulent boundary layer (Bradshaw, 1966). z/δ_{995} = 0.89, where δ_{995} is the boundary-layer thickness defined by the mean speed equal to 99.5% of the free-stream speed. Vertical axis is arbitrary. Center frequency of high-pass filter is shown in same nondimensional coordinates for a range of U (5–10 cm s^{-1}) and δ_{995} (10–20 m). The half-power bandwidth of this filter is also shown.

The amplitude of the high-pass velocity clearly varies in both space and time. This can be seen in both the raw high-pass velocity (Fig. 4a) and in the high-pass energy (Fig. 4b).

A 45 m thick, well-defined bottom mixed layer is present from 26 July to 1 August (Fig. 4c). The interior velocity during this period consists of a steady 7 cm s^{-1} current with approximately 3 cm s^{-1} (rms) internal-wave and tidal fluctuations.

Comparing the high-pass energy seen in Fig. 4b with the temperature field in Fig. 4c shows clouds of high-pass energy extending from below the array and intermittently filling the mixed layer. This can also be seen in Fig. 3 on 18–20 May, 30 May, 3 July, 11 July and 13–18 August. On 27 and 30 July (Fig. 4) even some of the small variations in mixed-layer height are reflected in the high-pass energy contours. On the assumption that the high-pass energy is a measure of boundary-layer turbulence, the turbulence is seen intermittently to fill the entire mixed layer.

Some fraction of the high-pass energy is clearly not due to boundary-layer turbulence. The clearest example of this is on 5 June, where the sharp frontlike density feature is accompanied by a peak in high-pass energy. Similar features can be seen clearly on

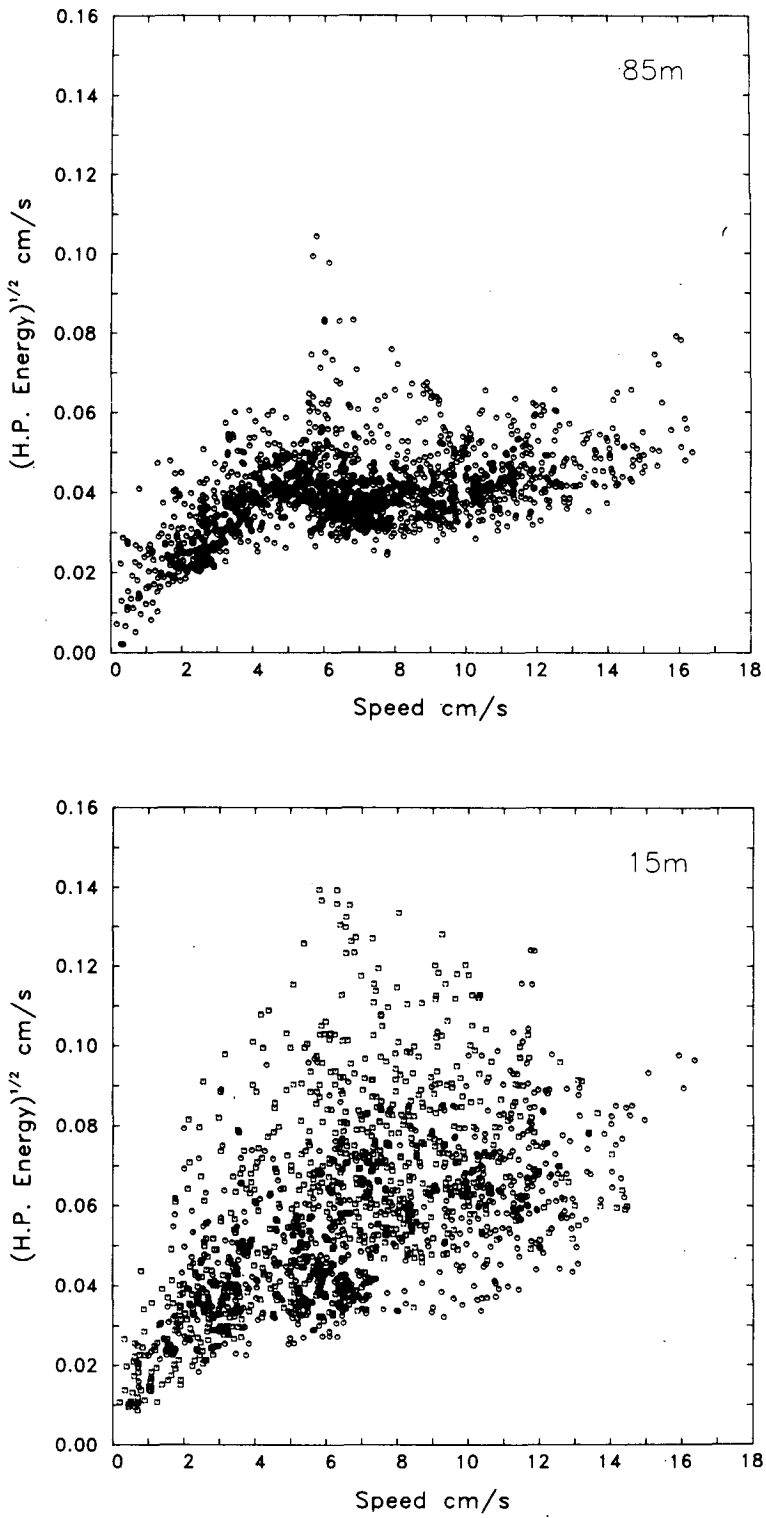

FIG. 2. Scatter plot of (3 h half-width half-cosine-filtered high-pass energy)$^{1/2}$ versus $(\bar{U} + \bar{V})^{1/2}$ with $\bar{U}$ and $\bar{V}$ 3 h half-width, half-cosine-filtered, eastward and northward velocity components. (a) 85 m instrument; this instrument is never in a mixed layer; (b) 15 m instrument; this instrument is commonly within mixed layers.

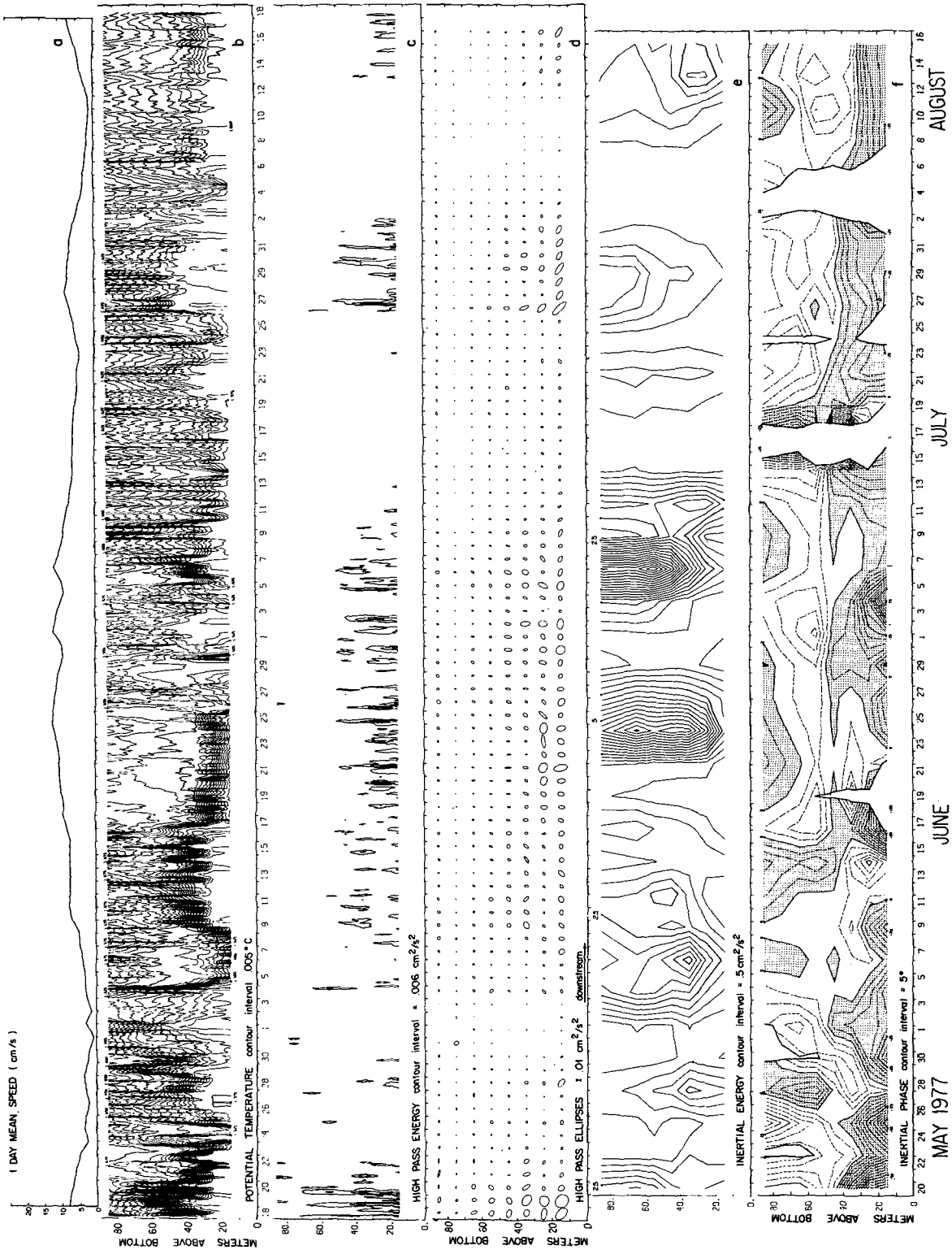

FIG. 3. Mean-velocity, temperature, high-pass-velocity and near-inertial-velocity structure for entire record. All figures plotted with same vertical and horizontal scales. Differences in start and stop times are due to differences in averaging. Data at 75 m are average of 85 m and 65 m data. (a) 1-day-mean speed at 15 m. (b) Contours of potential temperature filtered with a half-cosine filter of half-width 3 h. (c) Contours of filtered high-pass energy, plotted as a function of time and height off the bottom. The energy is formed from the individual high-pass velocity components and then filtered with a half-cosine filter of half-width 3 h. (d) Least-squares ellipses fitted to successive 24 h pieces of high-pass velocity. The ellipses are rotated so that high-pass-velocity fluctuations parallel to the 24 h-mean velocity are along the abscissa; velocity fluctuations perpendicular to the 24 h-mean velocity are along the ordinate. The size and orientation of these ellipses show the energy and directionality of the high pass velocity, respectively. (e) Contours of near-inertial clockwise energy computed as described in the text. (f) Contours of near-inertial phase of each instrument relative to the phase of the vertical-mean near-inertial velocity. Clockwise-leading phases are shaded. Phase contours are not shown when near-inertial energy is less than 0.25 $cm^2 s^{-2}$.

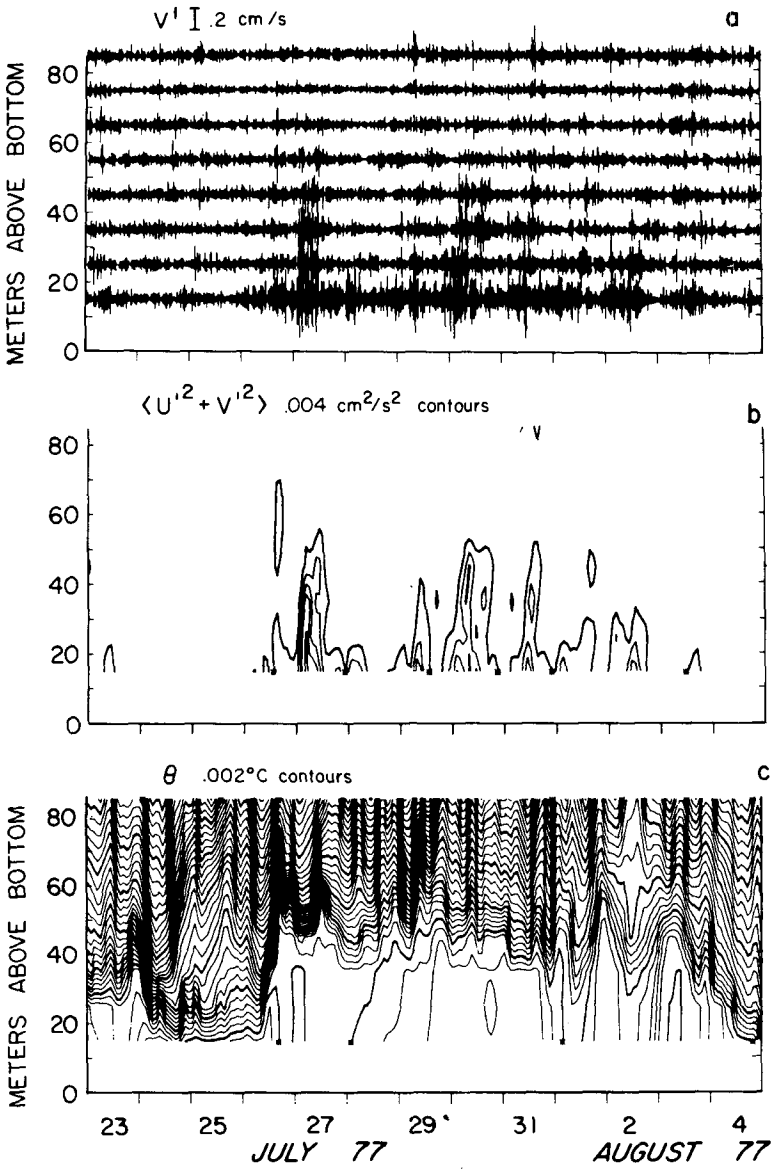

FIG. 4. High-pass velocity during a period of thick mixed layer. (a) High-pass northward velocity component for all seven instruments. Data from each instrument are plotted so that zero velocity corresponds to the height of that instrument off the bottom as shown on the left-hand axis. The data at 75 m are formed by averaging the 65 m and 85 m data. (b) Contours of filtered high-pass energy as in Fig. 3c. Notice how clouds of high-pass energy intermittently fill the mixed layer shown in (c). (c) Contours of potential temperature (as in Fig. 3b) with smaller contour interval.

9–15 June, and 19–20 May at the mixed-layer top, and in Fig. 4 on July 26. These velocity fluctuations are most likely due to Doppler-shifting of lower frequency velocities, associated with the density features, into the high-pass-velocity frequency band. Internal waves of this high frequency cannot exist, because of the weak stratification.

The mixed layer occurring during 9–15 June is interesting in that the high-pass energy does not extend to the mixed-layer top. It should also be noted that the large interior mixed regions, 17–25 June for example, correspond to low levels of high-pass energy.

Fig. 3d displays the directionality of the high-pass horizontal velocity. For each 24 h period a least-squares ellipse is fitted to the two components of high-pass velocity (Calman, 1978). These ellipses are plotted for each day and rotated so that a vertical

line corresponds to high-pass-velocity fluctuations oriented perpendicular to the 24 h mean velocity, while a horizontal line corresponds to fluctuations oriented parallel to the 24 h mean velocity. The concentration of high-pass energy within the mixed layer is clear. The velocity fluctuations are seen to align themselves roughly 45° clockwise of the mean velocity whenever the bottommost instrument is within a mixed layer. This can be seen on 18–21 May, May 28, 5–10 July and 12–16 August. McPhee and Smith (1976) observed no similar anisotropy in their turbulence data taken under the arctic ice.

Further discussion is postponed to Section 5 so that the observations of the near-inertial motions, which yield additional information on the boundary-layer turbulence, may be described.

4. Observed near-inertial-velocity structure

The average horizontal kinetic energy spectra shown by Armi and D'Asaro (1980, Fig. 10) indicate less near-inertial energy in the bottommost instruments than in the upper instruments. Similar near-bottom decreases in near-inertial energy have been observed by Kundu (1976), Hayes (1980) and Leaman (1976), and can clearly be seen in Fig. 5 of Weatherly and Wimbush (1980). In the following section the relation of this decrease to the bottom-mixed-layer structure is examined.

The 92-day velocity record from each instrument was broken into thirty-six 120 h long, 50% overlapping pieces. The near-inertial clockwise and anticlockwise components of velocity in each piece were found using a demodulation filter with center frequency of $^1/_{24}$ cph and a four-term Blackman-Harris window described by Harris (1978). Near the center frequency this window has a frequency response similar to that of a Hanning window with a 72 h piece. The side lobes, however, are much lower. Several other windows have been used and none of the results shown below depend critically on the particular window used.

a. Clockwise velocities

Fig. 5 shows a typical rotary energy spectrum. Most of the near-inertial energy is in clockwise motions. The analysis of the near-inertial velocity will thus concentrate on the clockwise component of motion. The clockwise near-inertial energy is vertically coherent, but varies significantly with time (Fig. 3e). There is clearly less near-inertial energy at the bottommost instruments. The height at which the energy decreases most rapidly, however, varies with time. Comparison of Fig. 3e with the potential temperature displayed in Fig. 3b shows that the height at which the inertial energy decreases most rapidly correlates

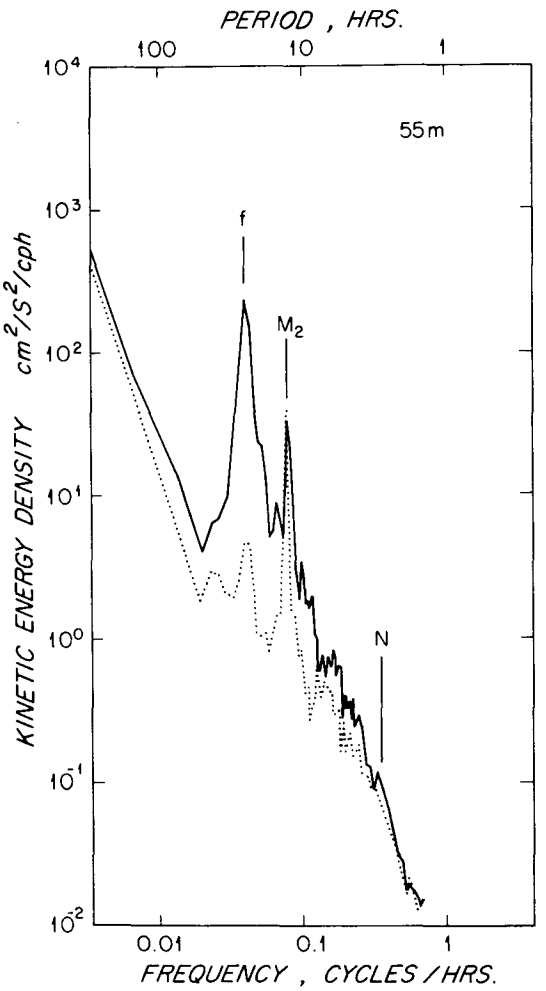

FIG. 5. Clockwise (solid) and anticlockwise (dotted) kinetic energy spectra for 55 m instrument. Each spectrum is the average of 13 Hanned overlapped pieces with higher frequencies band-averaged. The 95% confidence limits and the inertial (f), M_2 tidal, and approximate Väisälä (N) frequencies are shown.

with the height of the bottom mixed layer. For example, both the mixed-layer height and the height of maximum gradient are large on 20 May and 27–31 July. On 21–29 June and 12–16 August they both are small. The mixed layer top and the height of maximum gradient both decrease 20 m between 6 and 13 July. The major exception to this pattern occurs on 28 May, when a maximum in inertial energy is seen at the mixed-layer top. At this time, however, the mean velocity is small (Fig. 3a) and any turbulent-boundary-layer effects will thus be small. In general the mixed layer has less near-inertial energy than the interior, with the maximum gradient in energy occurring slightly above the top of the mixed layer.

Fig. 3f shows contours of the clockwise inertial phase at each level relative to the phase of the mean

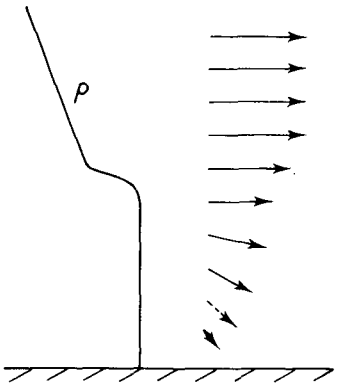

FIG. 6. Summary of observed near-inertial clockwise response. Arrows represent energy and phase of near-inertial clockwise velocity. Near-inertial energy decreases into the mixed layer, with the phase constant. Within the mixed layer the energy decreases slowly and the phase begins to lead the interior.

clockwise inertial velocity. Using the vertical mean as a reference rather than a particular level allows all levels to be treated identically. Regions of negative phase lead the mean and are shaded. The phases are not shown when the near-inertial energy is less than 0.25 $cm^2 s^{-2}$; they are quite noisy at these times.

The 15 m instrument leads in phase on the average, relative to the mean, and almost always relative to the 25 m instrument. The typical phase difference of 25° is significantly larger than any expected instrumental errors. Unlike the energy, the near-inertial phase exhibits large gradients within the bottom mixed layer, for example on 20–26 May, 3 June, 3 July and 10–15 August. Similar gradients do not generally appear above the mixed layer.

The phases computed here clearly show the apparent instrumental direction errors discussed in Section 1. The instruments at 55 and 65 m show a consistently positive (anticlockwise) phase, while the instruments at 85 and 45 m show a consistently negative clockwise phase. This effect is especially striking in late June and early July in the long tongues of negative phase at 45 m.

The phase structure of the near-inertial motions shows far less correlation with the density structure than does the energy. Although this may reflect the physics of the boundary layer it may also be due to the much higher noise level in the phase measurement. Spectral leakage from adjacent frequency bands affects phase more strongly than energy since these other frequencies, by definition, have rapidly varying phase with respect to the inertial frequency. The spectral leakage is also more severe for phase, being proportional to the filter transmission, rather than the transmission squared as for energy. Finally the phase, unlike horizontal kinetic energy, is sensitive to instrumental direction errors.

b. *Anticlockwise velocities*

The near-inertial anticlockwise motions are much less energetic than the clockwise motions. They do not show the strong correlation with density structure found for the clockwise motions; energy and phase diagrams similar to Figs. 3e and 3f are therefore not shown here.

Simple WKB internal wave theory predicts a ratio Γ of clockwise to anticlockwise energy of $\Gamma = (\sigma + f)^2/(\sigma - f)^2$ for $\sigma \approx f$ (Fofonoff, 1969). Fu (1981), accounting for the variability of f with latitude, finds this expression should be valid for $\sigma \geq 1.01f$. The value for Γ observed here is not consistent with internal wave theory. For example, Fig. 5 shows $\Gamma = 50$ at $\sigma = f$, corresponding to an internal wave frequency of $\sigma = 1.33f$. There is more anticlockwise energy than is predicted for internal waves. This suggests that much of the observed anticlockwise motion is not due to internal waves. Fu (1981) finds a similar excess of near-inertial anticlockwise energy in a large number of North Atlantic current-meter measurements.

c. *Summary*

Motions in the inertial-gravity-wave frequency band show a strong boundary-layer signal only near the inertial frequency. The near-inertial clockwise behavior is summarized in Fig. 6. Each arrow represents the amplitude and phase of the near-inertial clockwise velocity. The energy decreases near the top of the mixed layer with little phase change. Within the mixed layer the phase begins to lead, with the phase angle increasing downward. Extrapolation to the bottom indicates that the energy should drop to zero, with an unknown phase. The observed near-inertial anticlockwise velocities do not show a similarly simple pattern and they contain more energy than is predicted by simple internal wave theory.

D'Asaro (1982), using a scale analysis of the equations of motion, argues that the decrease in inertial energy within the mixed layer must be due to turbulent stresses. Since the entire mixed layer has less inertial energy, the turbulent stresses must extend throughout the mixed layer, when averaged over the space and time scales of the near-inertial motions. It is intriguing that the decrease in inertial energy occurs within the strongly stratified water above the mixed layer. This implies that stresses exist in the stratified water, perhaps as high-frequency, stress-carrying internal waves (Csanady, 1978).

5. Discussion

In this paper, two measures of boundary-layer turbulence are found: the high-pass velocity, which is sensitive to the turbulent velocity fluctuations, and

the near-inertial velocity deficit, which is sensitive to a particular component of the turbulent stress. Both indicate that the boundary-layer turbulence extends to the mixed-layer top, when averaged on the time scale of a day or longer. This conclusion is consistent with the radon-222 observations of Sarmiento (1978). Radon-222 is produced by the sediments and has a half-life of 3.8 days. It is present at significant concentrations up to the mixed-layer top, indicating that the entire mixed layer is turbulently mixed on a time scale of several days or less.

Boundary-layer turbulence in the outer part of the mixed layer, as measured by the high-pass velocity fluctuations, appears to be highly intermittent. Intermittency is expected in the outer part of two-dimensional turbulent boundary layers (Kovasznay *et al.*, 1970; Falco, 1977), with a period of roughly $2.5\delta/U$, with δ and U the boundary-layer thickness and free-stream speed respectively. Based on $\delta = 40$ m, $U = 7$ cm s^{-1}, the corresponding intermittency period for the benthic boundary layer is roughly 30 min. The observed intermittency, however, occurs with periods close to a day and is therefore a different phenomenon. Its period suggests that it is related to near-inertial forcing of the boundary layer, although no correlations between high-pass energy and the measured internal-wave-band velocities or accelerations have been found.

The observations presented here exclude neither mesoscale convergence nor turbulent entrainment as a mechanism for creating mixed layers thicker than $0.4\ u^*/f$. The observation of turbulence extending to the mixed-layer top suggests that some entrainment must continually be occurring, but the rate may be quite small. The steady boundary layer models that predict a boundary layer thickness of $0.4\ u^*/f$ may be inappropriate here because of the strong near-inertial motions present. A laminar Ekman layer is resonant at the inertial frequency (Greenspan, 1968) and grows indefinitely. A turbulent boundary layer should be subject to the same resonance. Weatherly *et al.* (1980), using a turbulence-closure model of the benthic boundary layer, find that the addition of inertial forcing results in a doubling of the mixed-layer height. The strong intermittency of the high-pass energy in Fig. 3, on a roughly inertial time scale, also suggests that forcing at inertial and tidal frequencies is important.

It is also possible that convergence and divergence of the boundary layer, induced by the overlying mesoscale eddies, may thicken the mixed layer. Turbulent entrainment should be much more rapid for thin mixed layers. A boundary layer thinned by divergence and then thickened by an equivalent amount of convergence will achieve a greater thickness than if no divergence had occurred, on account of rapid entrainment when the layer was thin. The continued mixing of mixed layers to thicknesses of at least 45 m, as hypothesized here, will aid in the mesoscale thickening process, by maintaining the thickened mixed layers and inhibiting their destruction by mean vertical shears.

Acknowledgments. I would like to thank Laurence Armi for innumerable discussions and many valuable suggestions and an anonymous reviewer for his constructive and extensive criticisms of the original manuscript.

This research was supported by the Office of Naval Research under Contract N00014-76-C-0197, NR 083-400 and the National Science Foundation under Grant OCE 76-81190 through the Woods Hole Oceanographic Institution. Partial support was provided by a National Science Foundation graduate fellowship. Publication costs were supported by the Office of Naval Research under Contracts N00014-80-C-0252 through the Applied Physics Laboratory, University of Washington and N00014-80-C-0440 through the Scripps Institution of Oceanography. This is contribution number 4876 from the Woods Hole Oceanographic Institution.

REFERENCES

Armi, L., 1977: The dynamics of the bottom boundary layer in the deep ocean. *Bottom Turbulence, Proceedings of the 8th International Liège Colloquium on Ocean Hydrodynamics*, J. C. J. Nihoul, Ed., Elsevier, pp. 153–164.

——, and R. C. Millard, 1976: The bottom boundary layer of the deep ocean. *J. Geophys. Res.*, **81,** 4983–4990.

——, and E. D'Asaro, 1980: Flow structures of the benthic ocean. *J. Geophys. Res.*, **85,** 469–483.

Arya, S. P. S., 1972: The critical condition for the maintenance of turbulence in stratified flows. *Quart. J. Roy. Meteor. Soc.*, **98,** 264–273.

Biscaye, P. E., and S. L. Eittreim, 1977: Suspended particulate loads and transports in the nepheloid layer of the abyssal Atlantic Ocean. *Mar. Geol.*, **23,** 155–172.

Bowden, K. F., 1978: Physical problems of the benthic boundary layer. *Geophys. Surv.*, **3,** 255–296.

Bradshaw, P., 1966: The turbulence structure of equilibrium boundary layers. NPL Aeronautical Report, No. 1184, Great Britain.

Bryden, H. L., 1976: Horizontal advection of temperature for low frequency motions. *Deep-Sea Res.*, **23,** 1165–1174.

Caldwell, D. R., 1976: Fine-scale temperature structure in the bottom mixed layer on the Oregon shelf. *Deep-Sea Res.*, **23,** 1025–1035.

——, C. W. van Atta and K. N. Helland, 1972: A laboratory study of the turbulent Ekman layer. *Geophys. Fluid Dyn.*, **3,** 125–160.

Calman, J., 1978: On the interpretation of ocean current spectra. Part I: The kinematics of three-dimensional vector time series. *J. Phys. Oceanogr.*, **8,** 627–643.

Csanady, G. T., 1967: On the "Resistance Law" in a turbulent Ekman layer. *J. Atmos. Sci.*, **24,** 467–471.

——, 1978: Turbulent interface layers. *J. Geophys. Res.*, **83,** 2329–2342.

D'Asaro, E., 1980: Structure and dynamics of the benthic boundary layer above the Hatteras Abyssal Plain, Ph.D. thesis, MIT/WHOI Joint Program in Oceanography.

——, 1981: Absorption of internal waves by the benthic boundary layer. *J. Phys. Oceanogr.*, **12,** 323–336.

Falco, R. E., 1977: Coherent motions in the outer region of turbulent boundary layers. *Phys. Fluids,* **20,** 5124–5132.

Fofonoff, N. P., 1969: Spectral characteristics of internal waves in the ocean. *Deep-Sea Res.*, **16**(Suppl), 59–71.

Fu, L. L., 1981: Observations and models of inertial waves in the deep ocean. *Rev. Geophys. Space Phys.*, **19,** 141–170.

Greenspan, H. P., 1968: *The Theory of Rotating Fluids.* Cambridge University Press, 327 pp.

Hamming, R. W., 1977: *Digital Filters.* Prentice-Hall, 256 pp.

Harris, F. J., 1978: On the use of windows for harmonic analysis with the discrete Fast Fourier Transform. *Proc. IEEE,* **66,** 51–83.

Hayes, S. P., 1980: The bottom boundary layer in the eastern tropical Pacific. *J. Phys. Oceanogr.*, **10,** 315–329.

Hinze, J. O., 1959: *Turbulence.* McGraw-Hill, 586 pp.

Kovasznay, L. S., V. Kibens and R. N. Blackwelder, 1970: Large scale motion in the intermittent region of a turbulent boundary layer. *J. Fluid Mech.*, **41,** 283–325.

Kundu, P. K., 1976: An analysis of inertial oscillations observed near the Oregon coast. *J. Phys. Oceanogr.*, **6,** 879–893.

Leaman, K. D., 1976: Observations on the vertical polarization and energy flux of near-inertial waves. *J. Phys. Oceanogr.*, **6,** 894–908.

McCullough, J. R., 1975: Vector averaging current meter speed calibration and recording techniques. Woods Hole Oceanographic Institution, Tech. Rep. WHOI-75-44.

McPhee, M. G., and J. D. Smith, 1976: Measurements of the turbulent boundary layer under pack ice. *J. Phys. Oceanogr.*, **6,** 696–711.

Millikan, C. B., 1939: A critical discussion of turbulent flows in channels and circular tubes. *Proceedings of the 5th International Congress on Applied Mechanics,* Wiley, pp. 386–392.

Sarmiento, J., 1978: A study of the mixing of the deep sea based on STD, radon-222 and radium-228 measurements. Ph.D. thesis, Columbia University.

Spencer, A., E. D'Asaro and L. Armi, 1981: The Benthic Boundary Layer Experiment on the Hatteras Abyssal Plain: Current and temperature observations. Woods Hole Oceanographic Institution, Tech. Rep. WHOI-1981-12.

Thompson, R.O.R.Y., 1973: Stratified Ekman boundary layer models. *Geophys. Fluid Dyn.*, **5,** 201–210.

Turner, J. S., 1973: *Buoyancy Effects in Fluids.* Cambridge University Press, 368 pp.

Weatherly, G. L., 1975: A numerical study of time-dependent turbulent Ekman layers over horizontal and sloping bottoms. *J. Phys. Oceanogr.*, **5,** 288–299.

——, and P. O. Niiler, 1974: Bottom homogenous layers in the Florida Current. *Geophys. Res. Lett.*, **1,** 316–319.

——, and P. J. Martin, 1978: On the structure and dynamics of the ocean bottom boundary layer. *J. Phys. Oceanogr.*, **8,** 557–570.

——, and M. Wimbush, 1980: Near-bottom speed and temperature observations on the Blake-Bahama Outer Ridge. *J. Geophys. Res.*, **85,** 3971–3981.

——, S. L. Blumsack and A. A. Bird, 1980: On the effect of diurnal tidal currents in determining the thickness of the turbulent Ekman bottom boundary layer., *J. Phys. Oceanogr.*, **10,** 297–300.